# Brillouin light-scattering experiments on exchange-coupled ultrathin bilayers of iron separated by epitaxial copper (001)

J. F. Cochran, J. Rudd, W. B. Muir,* B. Heinrich, and Z. Celinski
*Physics Department, Simon Fraser University, Burnaby, British Columbia, Canada V5A 1S6*
(Received 9 February 1990)

The magnetic properties of bilayers of bcc Fe(001) separated by bcc Cu(001) films of variable thickness have been investigated by means of Brillouin light scattering. For copper thicknesses less than 9 monolayers (ML) the coupling between the iron films was found to be ferromagnetic; for thicknesses between 9 and 12 ML the coupling was found to be antiferromagnetic. The data are compared with the results of a model calculation that assumes a uniform static magnetization across each film: The magnetizations of the two films, $M_A$ and $M_B$, are assumed to be coupled by an interaction energy of the form $J\mathbf{M}_A\cdot\mathbf{M}_B/(|M_A||M_B|)$, where $J$ is a surface energy. For small applied fields and for antiferromagnetic coupling the magnetizations in the films need not be parallel. The magnetic-field dependence of frequencies calculated using this model display features that are similar to the observations.

## INTRODUCTION

It has recently been discovered that single-crystal trilayers can be prepared by means of molecular-beam epitaxy in which two ultrathin iron layers are separated by a uniform layer of body-centered cubic cooper.[1] Body-centered cubic copper [bcc Cu(001)] grows layer by layer on the (001) surfaces of ultrathin body-centered cubic iron films [bcc Fe(001)] that have been grown on the (001) surface of silver; conversely, bcc Fe(001) films grow layer by layer on the bcc Cu(001) surfaces. This has made it possible to prepare single-crystal sandwiches in which two ultrathin iron layers are separated by a uniform bcc Cu(001) layer whose thickness may be varied at will. The question then arises as to how the strength of the exchange coupling between the two ferromagnetic films is modified by the presence of the intervening copper layer. It is clear that this exchange coupling must approach a value corresponding to the exchange interaction in bulk iron in the limit of zero copper thickness. It is equally clear that this exchange coupling must approach zero for very thick copper layers. We have concluded,[1] on the basis of ferromagnetic-resonance (FMR) experiments, Brillouin light-scattering (BLS) experiments, and surface magneto-optic Kerr-effect (SMOKE) measurements, that the interlayer exchange interaction is strongly ferromagnetic for copper thicknesses of 9 monolayers (ML) or less, but that the interaction becomes antiferromagnetic for thicknesses of copper between 9 and 13 ML. It is the purpose of this report to provide a more detailed description of the BLS results than was possible in the original publication.[1] We also wish to describe a model calculation with which to compare the measured BLS frequencies and scattered light intensities. The model is an extension of the one used previously to discuss FMR measurements on bilayers of nickel and iron.[2] It is assumed that the two ferromagnetic films are uniformly magnetized across their thickness and that they interact with each other through an interlayer exchange-coupling energy of the form used by Hoffman, Stankoff, and Pascard,[3] i.e.,

$$F_x = J\mathbf{M}_A\cdot\mathbf{M}_B/(|M_A||M_B|)\ , \tag{1}$$

where $\mathbf{M}_B,\mathbf{M}_B$ are the magnetization densities of the two ferromagnetic layers.[4] This model is equivalent to the well-known model of exchange-coupled sublattices.[5] One expects two eigenmodes for this model: the acoustic mode in which the magnetizations of the two films oscillate in phase around their equilibrium orientation and the optical mode in which the magnetizations oscillate out of phase. The previous discussion[2] of this model considered only the case in which the equilibrium magnetizations were parallel. However, for antiferromagnetic coupling between the two films their equilibrium magnetizations will, for a range of applied magnetic field, be neither parallel nor antiparallel. We have therefore extended the model calculation to include nonparallel equilibrium magnetizations. We have also included an estimate of the dipole-dipole interaction between the spin waves in the two films. This interaction is negligible for the eigenmodes which are measured in an FMR experiment. In the FMR experiment the excursions of the magnetizations from equilibrium are uniform in the plane of the films: the resulting surface magnetic pole densities are therefore uniform in the plane and produce no magnetic fields outside each film. Thus there is no magnetic interaction between the two magnetic layers. The eigenmode frequencies that are measured using BLS, on the contrary, correspond to an in-plane traveling wave characterized by a wave vector, $q$, which is related to the wavelength of the light used, to its angle of incidence, and to the angle at which the scattered light is measured. The in-plane variation of the surface magnetic pole density that results from the in-plane variation of the magnetization components generates an external magnetic field that couples the magnetizations in the two films even in the absence of any interlayer exchange coupling.[6,7] As will be shown later, the magnetic-field dependencies of

 

the coupled bilayer magnetic mode frequencies observed by means of BLS exhibit features that can be understood on the basis of the preceding simple model of exchange-coupled magnetizations. The magnetic-field dependencies of the intensities of the scattered light as predicted by the simple model are not in good agreement with the BLS observations at small values of the applied field. The origin of this discrepancy is not known. It may be that a more complex model is required that takes into account the spatial variation of the magnetization density across the thickness of each film.

## EXPERIMENTAL DETAILS

### A. Film growth

Growth of the epitaxial thin films was carried out in a Physical Electronics molecular-beam epitaxy system (Φ MBE-400). This system was equipped with a reflection high-energy electron diffraction (RHEED) apparatus, and an angularly resolved double-pass cylindrical-mirror analyzer (CMA) for Auger-electron spectroscopy (AES) and x-ray photoelectron spectroscopy (XPS). The quality and character of the film growth was monitored during deposition by means of RHEED: the intensity of the RHEED specular spot was measured by means of a collection lens and a photomultiplier tube.

The ultrathin films were grown on the (001) face of a bulk silver single crystal 15 mm in diameter and approximately 3 mm thick spark-cut from a silver single-crystal boule. The (001) axis was parallel with the normal to the specimen surface within $\frac{1}{4}°$. The substrate surface was ground and polished mechanically. It was given a final electropolish using a cyanide-free solution.[8] This treatment produced a strain-free, smooth, mirrorlike surface. The silver substrate surfaces were cleaned and recrystallized using several cycles of argon ion sputtering (2 keV) at an elevated temperature. The first sputtering period was performed at 500 °C. After approximately 5 min the sputtering was stopped and the temperature of the substrate was allowed to fall slowly to 450 °C, whereupon sputtering was resumed for a few minutes. This procedure was repeated several times: the final annealing temperature used was 350 °C.

Iron films were deposited by evaporation from a tungsten wire. The copper was evaporated from a resistively heated tantalum boat. During deposition the substrate temperature was maintained at 300 K. Deposition rates, approximately 2 ML per min, were measured by means of the oscillations observed in the RHEED specular spot intensity.[2] It is estimated that thicknesses were accurate to within $\pm\frac{1}{8}$ monolayer (ML). Further details of the crystal growth can be found in Ref. 2.

It was known from previous studies[2,9–11] that bcc Fe(001) films grow layer by layer on a singular fcc Ag(001) surface: the bcc lattice spacing matches the fourfold hollows on the silver (001) surface when the iron cubic axes are rotated 45° with respect to the silver cubic axes. The slow deposition of Cu on a bulk Fe(001) surface, 1 ML per 3 min, produced films of poor quality according to Wang *et al.*:[12] low-energy electron diffraction (LEED) studies showed that the ordered portions of the film were formed in a distorted bcc structure. However, the use of a faster growth rate ($\sim$2 ML per min) on an ultrathin bcc Fe(001) template produced high-quality single-phase Cu(001) films.[1] The good quality of the Cu(001) films was attested by the narrow RHEED streaks and by the large-amplitude RHEED oscillations that were observed during the copper deposition.[1] The resulting copper films on Fe(001) exhibited RHEED streak separations which were approximately 1.2% smaller than the Fe(001) streak separations; this means that the in-plane copper lattice spacing was approximately 1.2% larger than the iron lattice spacing.[1] RHEED is generally not sensitive to the vertical lattice spacing. The anti-Bragg angle [RHEED(amp.osc.min.)=0] for Fe growth on a Fe(001) whisker substrate was very close to the anti-Bragg condition for bcc Cu grown on Fe(001). That implies that the vertical interference conditions are nearly the same for both cases.[13] One can therefore argue that the Cu(001) overlayers grow in a nearly perfect bcc structure. Angular resolved XPS measurements[14] show that the vertical distortion of bcc Cu(001) grown on Ag(001) substrates is small. Ultimately vertical distortions and surface relaxations of bcc Cu(001) grown on ultrathin Fe(001) surfaces will be determined from LEED studies. In this work the term "bcc structure" will be used to describe the growth of the first 10 ML of Cu(001) on Fe(001) without resolving the question of tetragonality. One could avoid possible controversy by describing our structure as a body-centered tetragonal (bct) rather than as bcc. However, on the basis of current evidence, we believe that the tetragonal distortion is small. Hopefully, future structural studies will clarify the extent to which the vertical spacing corresponding to the square mesh is distorted from that for simple bcc stacking.

The copper layers maintained the same in-plane symmetry as the iron layers for 10–11 ML; for greater thicknesses the films underwent a structural modification in which the {10} azimuths developed two additional symmetrically spaced streaks, and the {11} azimuths developed superlattice streaks that did not appear to be commensurate with the lattice periodicity (see Fig. 1 of Ref. 1). The bcc Fe(001) overlayers grew in a good layer-by-layer mode even when deposited upon lattice modified Cu(001) films[1] (i.e., copper films thicker than 10 ML).

All the structures that we studied were capped with 20 ML of Au(001). This gold coverlayer protected the films against oxidation when they were removed from the ultrahigh vacuum system for the FMR and BLS measurements.

### B. BLS measurements

Brillouin light-scattering measurements were carried out on thin-film specimens using approximately 100 mW of the 5145 Å line from an argon ion laser, and in the backscattering configuration for which the angle of incidence of the light is the same, on average, as the collection angle for the scattered light.[15–17] The scattered light was analyzed using a Sandercock tandem interferometer[15] in a four-pass plus two-pass configuration.

The specimens were mounted between the poles of an electromagnet such that the magnetic field was oriented parallel with the plane of the surface. The plane of incidence of the light was oriented perpendicular to the magnetic field. A polarizing beam-splitter cube[18] was used to discriminate against scattered light having the same polarization as the incident light. This reduced the background intensity of light scattered from surface defects, but allowed light scattered from magnetic excitations to reach the interferometer with practically no attenuation. Otherwise the apparatus used was very similar to that described by Sandercock.[15]

All BLS measurements were carried out at room temperatures (approximately 295 K). In all cases the linewidth of the Stokes and anti-Stokes lines appeared to be determined by the instrumental resolution rather than by the intrinsic linewidth of the magnetic excitations that were responsible for the scattering. The smallest free spectral range which was used was 12 GHz: the instrumental linewidth for this free spectral range was found to be approximately 0.6 GHz full width at half maximum.

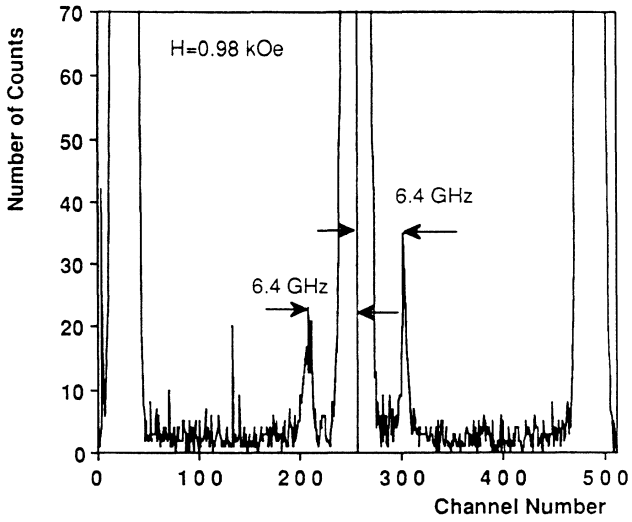


FIG. 1. Scattered-light intensity vs channel number for the magnetic monolayer specimen $S2$ (Table I) obtained using 5154-Å light in the backscattering configuration. The free spectral range used was 30 GHz and 452 channels=60 GHz. The dwell time per channel was 1 msec. The data were collected using 500 sweeps. The externally applied magnetic field was 0.98 kOe.

## RESULTS

BLS data were obtained for two specimens consisting of a single iron film grown on Ag(001) and covered with bcc Cu(001), and for four specimens consisting of two bcc Fe(001) films separated by a bcc Cu(001) spacer layer. The composition of these films is listed in Table I. The objective was to measure the magnetic properties of the individual 5- and 10-ML iron films ($S1$ and $S2$ of Table I), and to use those magnetic properties, along with the theory to be described below, to extract values for the interlayer exchange-coupling parameter for the magnetic bilayer systems (specimens $T1$ to $T4$ of Table I).

### A. The single iron films $S1$ and $S2$

A spectrum obtained from specimen $S2$ [5 ML of bcc Fe(001)] is shown in Fig. 1 for a magnetic field of 0.98 kOe applied along an easy fourfold cubic axis. The intensities of the Stokes and anti-Stokes lines due to light scattered from magnetic excitations in the iron film were weak but well defined. Data were obtained for magnetic fields ranging from 0.49 to 6.73 kOe—the practical upper limit placed on the magnetic field for the 30-GHz free spectral range used because the magnon peaks began to merge with the much more intense Rayleigh peaks. No hysteresis was observed, within experimental uncertainty, as the applied field was cycled to the maximum available ($\pm 10$ kOe) through zero field.

For $\lambda_0=5145$ Å light incident at $\theta=45°$, and for the backscattering geometry, the frequency-shifted light has been scattered from magnons whose spatial variation in the plane of the film is specified by the wave vector

$$q=(2\pi/\lambda_0)(2\sin\theta)=1.73\times10^5\ \mathrm{cm}^{-1}\ .$$

For films 5 and 10 ML thick (corresponding to $d=7.15$ and 14.3 Å) the product $qd$ is very small ($qd=0.025$ for the 10-ML film) and therefore the frequency of the lowest magnon mode is essentially the same as the frequency of the homogeneous mode:[16,17] it is the frequency of the homogeneous mode that is measured in an FMR experiment. This neglects a small correction for the intralayer

TABLE I. List of specimens measured by means of Brillouin light scattering (backscattering of 5145-Å laser light incident at 45°). The notation (Ag/5.0Fe/11.6Cu/10.3Fe/20Au) means that 5.0 monolayers (ML) of bcc Fe(001) were grown on a bulk single-crystal Ag(001) surface, followed by the deposition of 11.6 ML of bcc Cu(001) and by 10.3 ML of bcc Fe(001); finally, a protective coverlayer was deposited consisting of 20 ML of epitaxial fcc Au(001).

| Specimen | Composition |
|---|---|
| $S1$ (one magnetic layer) | (Ag/9.0Cu/10.0Fe/20Au) |
| $S2$ (one magnetic layer) | (Ag/5.0Fe/12.0Cu/20Au) |
| $T1$ (two magnetic layers) | (Ag/5.0Fe/6.0Cu/11.0Fe/20Au) |
| $T2$ (two magnetic layers) | (Ag/9.5Fe/8.7Cu/5.0Fe/20Au) |
| $T3$ (two magnetic layers) | (Ag/5.0Fe/11.6Cu/10.3Fe/20Au) |
| $T4$ (two magnetic layers) | (Ag/4.8Fe/12.6Cu/9.0Fe/20Au) |

exchange, $2Aq^2/M_s$, due to the spatial variation of the magnetization in the plane of the film ($A$ is the exchange stiffness parameter and $M_s$ is the saturation magnetization). The correction for room-temperature iron is approximately 70 Oe corresponding to 0.2 GHz; shifts of this magnitude are smaller than the resolution of the Fabry-Perot interferometer—approximately 0.8 GHz full width at half maximum for a 30-GHz free spectral range. Data obtained for the 5- and 10-ML single iron films were therefore analyzed using the well-known FMR formula for fields directed along a cubic axis:[2]

$$[\omega/\gamma]^2=[H+(2K_1/M_s)][H+4\pi M_{\text{eff}}+(2K_1/M_s)] , \tag{2}$$

where $H$ is the applied magnetic field, $K_1$ is the cubic magnetocrystalline anisotropy constant, $\gamma=g|e|/2mc$ is the spectroscopic splitting factor, and $4\pi M_{\text{eff}}$ is the effective magnetization density. The effective magnetization density differs from the actual magnetization density, $4\pi M_s$, due to the presence of a uniaxial magnetic energy associated with the broken cubic symmetry at the surfaces of the film.[19] Such a surface-energy term becomes very important for thin films because it contributes an effective magnetic field that is inversely proportional to $d$, the thickness of the layer:[9,19,20]

$$4\pi M_{\text{eff}}=4\pi M_s-(2K_u/dM_s) , \tag{3}$$

where $K_u$ is the uniaxial surface anisotropy constant which gives a surface energy $E_s=K_u(M_p/M_s)^2$ ergs/cm$^2$ and $M_p$ is the magnetization component perpendicular to the surface.

We had hoped that the BLS data (a total of 12 field values equally spaced between 0 and 7 kOe), together with the FMR data point at 36.3 GHz, would enable us to deduce unambiguous values for the three parameters associated with Eq. (2): $g$, $4\pi M_{\text{eff}}$, and $2K_1/M_s$. However, given a particular value of $g$ ranging from 2.0 to 2.2 we could adjust the other two parameters to obtain a satisfactory fit of Eq. (2) to the data. We have, therefore, used a value $g=2.09$. This value of $g$ has been measured for ultrathin films of bcc Fe(001) grown on Ag(001) and covered with Au(001), and ranging in thickness from 5 to 14 ML.[9,10,20] Magnetic parameters so determined are listed for the 5- and 10-ML iron films in Table II.

It should, perhaps, be mentioned explicitly that we expected to observe only one magnetic mode for the single ultrathin iron films, that corresponding to the homogeneous mode. The mode next highest in frequency, corresponding to a standing spin-wave mode having a wavelength of twice the film thickness, was expected to occur at a frequency that was very much larger than the maximum free spectral range (200 GHz) available in our apparatus. For example, the first standing spin-wave frequency for a 10-ML iron film occurs at 3300 GHz corresponding to an effective field $(2A/M_s)(\pi/d)^2$.

### B. The magnetic bilayer films $T1-T4$

The magnetic bilayer films corresponding to the thinnest copper layers separating the iron films ($T1$ and $T2$ of Table I) behaved very much like a single iron film: they exhibited a single FMR resonance line at 36.3 GHz and a single pair of scattered-light peaks in the BLS experiments. A careful search was carried out over the frequency range 2–200 GHz but revealed only a single pair of Stokes anti-Stokes lines. It is estimated that a second mode having an intensity as small as 2% of the observed mode could have been detected (see Fig. 2). It is natural to assume that the observed mode corresponded to the low-frequency acoustic mode for two iron films coupled through a ferromagnetic exchange interaction that was sufficiently strong to drive the frequency, or the intensity, of the optical magnetic mode[17] out of the range of our apparatus.

The magnetic sandwiches corresponding to the thicker copper spacer layers ($T3$ and $T4$ of Table I) exhibited two pairs of Stokes anti-Stokes lines in the BLS experiments, and they also exhibited two 36.3-GHz FMR resonance signals.[1] The FMR and BLS data were found to be in excellent agreement. BLS data for specimen $T3$ are shown in Fig. 3. Stokes and anti-Stokes frequencies were found to be the same within the experimental uncertainty except for fields less than 1 kOe. The two points at each field for the low-frequency branch shown in Fig. 3 were obtained using a 12-GHz free spectral range, and show very clearly a difference of approximately 1.2 GHz in frequency between the Stokes and anti-Stokes lines for fields less than 1 kOe (see Fig. 4). A shift in frequency between Stokes and anti-Stokes lines at small magnetic fields is ex-

TABLE II. Room-temperature magnetic parameters for the individual iron films 10 monolayers (ML) and 5 ML thick (specimens $S1$ and $S2$ of Table I) deduced from combined BLS and FMR data using Eq. (2). Values of $4\pi M_{\text{eff}}$ and $2K_1/M_s$ have been obtained using $g=2.09$. The anisotropy constants $K_1$ and $K_u$ have been calculated assuming a magnetization density $4\pi M_s=21.55$ kOe, the value for room-temperature bulk bcc iron. $K_u$ has been calculated using Eq. (3) of the text. For bcc Fe(001) 1 ML=1.43 Å.

| Specimen | Thickness (ML) | $4\pi M_{\text{eff}}$[a] (kOe) | $2K_1/M_s$[a] (kOe) | $K_1$ (ergs/cm$^3$) | $K_u$ (ergs/cm$^2$) |
|---|---|---|---|---|---|
| $S1$ | 10.0 | 13.53 | 0.259 | $2.22\times10^5$ | 0.98 |
| $S2$ | 5.0 | 3.08 | 0.113 | $0.97\times10^5$ | 1.13 |

[a]These values of $4\pi M_{\text{eff}}$ and $2K_1/M_s$ are the same as those listed in Ref. 1, and were deduced from

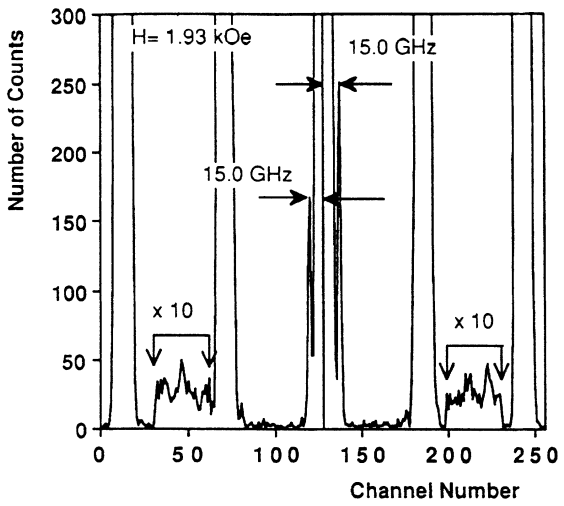


FIG. 2. Scattered-light intensity vs channel number for the magnetic monolayer specimen $T1$ (Table I) obtained using 5145-Å light in the backscattering configuration. The free spectral range used was 100 GHz and 226 channels=400 GHz. The dwell time per channel was 2 msec except for the intervals between the outer Rayleigh peaks indicated on the figure for which the dwell time per channel was increased to 20 msec. The data were collected using 868 sweeps. The externally applied magnetic field was 1.93 kOe.

pected for magnetic bilayers having oppositely oriented magnetizations.[21]

The variation of the scattered-light intensities with magnetic field was strong at low fields, see Fig. 5. Intensities are not very reproducible because any small motion, of the order of a wavelength of light, of the specimen relative to the collecting lens causes a large change in the intensity of the scattered light collected. However, the data

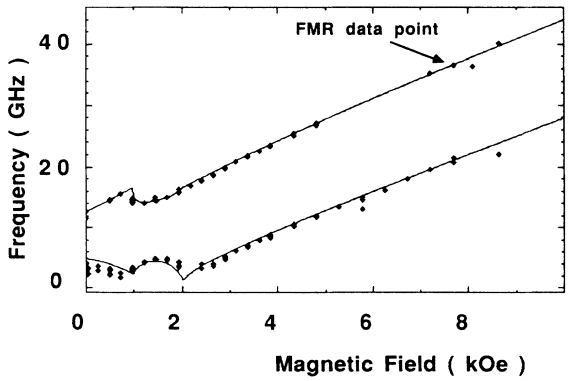


FIG. 3. The variation of magnetic excitation frequencies with applied magnetic field observed using the magnetic bilayer specimen $T3$ (Table I). This bilayer specimen exhibited two magnon frequencies at each value of the magnetic field. The solid lines were calculated using the theory described in the text. The double data points shown for the low-frequency branch, and for small magnetic fields, are a consequence of the unequal frequencies exhibited by the Stokes and anti-Stokes lines. The Stokes and anti-Stokes frequencies were the same, within experimental uncertainty, for all measurements corresponding to the high-frequency branch.

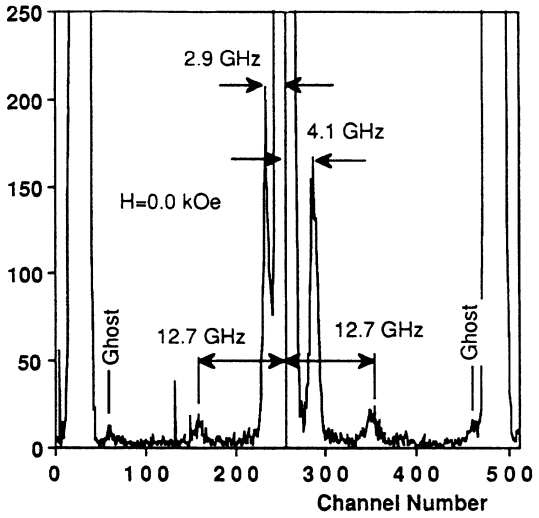


FIG. 4. Scattered-light intensity vs channel number for the magnetic monolayer specimen $T3$ (Table I) obtained using 5145-Å light in the backscattering configuration and zero applied magnetic field. The free spectral range used was 30 GHz and 454 channels=60 GHz. The dwell time per channel was 1 msec. The data were collected using 500 sweeps. This figure shows that the intensities of the low-frequency lines are stronger than the intensities of the high-frequency lines. It also illustrates the slightly different frequencies that were observed for the low-frequency Stokes and anti-Stokes lines: the frequency difference is approximately 1.2 GHz.

shown in Fig. 5 were obtained for both an increasing and a decreasing magnetic-field sweep and indicated very clearly that the intensity corresponding to the high-frequency mode reached a maximum at approximately 2 kOe, and that the intensity of the low-frequency mode fell off with increasing magnetic field. For fields larger than 3 kOe the ratio of the BLS intensities for the two modes was found to be approximately 3:1, with the high-frequency mode having the greater intensity.

Similar data, but less extensive, were obtained for the magnetic bilayer specimen $T4$ of Table I. The magnetic-field dependencies of the two observed frequencies and their intensities were similar to the data shown in Figs. 3 and 5. The observation of two frequencies, and their magnetic-field dependencies, is consistent with the hypothesis that the two iron films were coupled through an antiferromagnetic exchange interaction, as will be shown later. No hysteresis effects were observed in any of the magnetic bilayer films as the applied field was repeatedly cycled from $+10$ to $-10$ kOe.

## MODEL FOR A PAIR OF EXCHANGE-COUPLED THIN FILMS

Two cubic magnetic thin films, $A$ and $B$, having their surfaces parallel with the $xz$ plane, and characterized by thicknesses $d_A$ and $d_B$, are separated by a nonmagnetic spacer layer of thickness $d$ (see Fig. 6). An external magnetic field is applied along the $z$ axis. It is assumed that the coordinate axes are parallel with the cubic axes (easy

axes) for both magnetic films. It is further assumed that the equilibrium magnetization densities, $M_A$ and $M_B$, are uniform within a given film. This model has been treated by a number of authors for the case in which the equilibrium magnetizations are parallel with the direction of the applied magnetic field.[21–25] We wish to consider explicitly cases in which the directions of these equilibrium densities may not be parallel with the applied magnetic field and may be different for each film. The direction of the equilibrium magnetization density in each film depends upon the interplay between torques due to (i) the external magnetic field $H$, (ii) the volume magnetocrystalline anisotropy energy $F_c$, (iii) internal demagnetizing fields due to surface poles, (iv) a uniaxial surface energy term, and (v) the exchange coupling between the two films (see Refs. 26 and 27, for example). The pole fields generated by div**M** are confined entirely within each film for a uniform magnetization density, therefore dipole-dipole coupling between the two films play no role in determining the directions of their equilibrium magnetizations. However, dipole-dipole coupling will be taken into account in calculating the normal modes of the system that describe the magnetization oscillations around the equilibrium configurations.

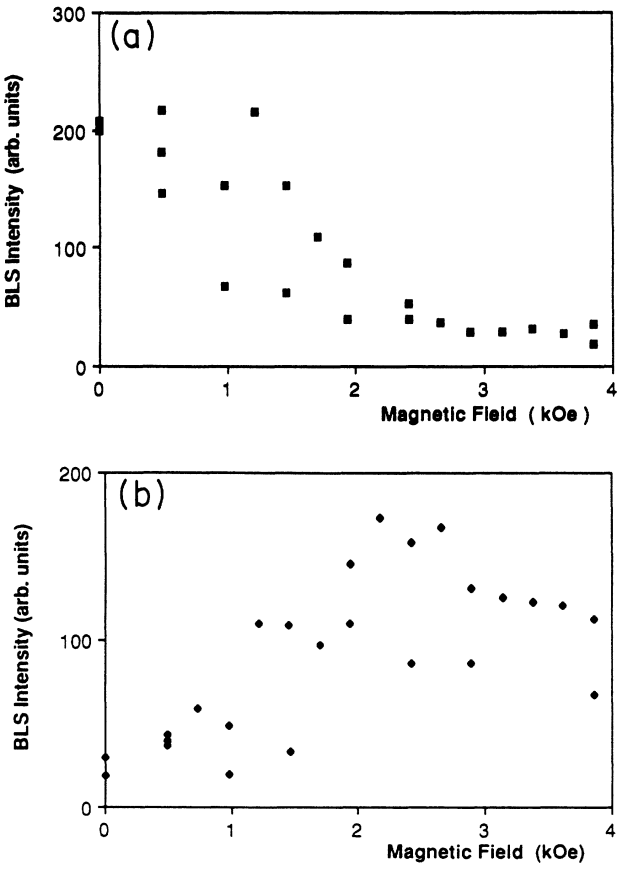


FIG. 5. Magnetic-field dependence of the BLS intensities observed using specimen $T3$ (Table I): the magnetic-field dependence of the corresponding frequencies is shown in Fig. 3. (a) field dependence for the low-frequency branch intensities; (b) field dependence for the high-frequency branch intensities.

Let the equilibrium positions of the magnetizations be specified by the angles $\theta_A$ and $\theta_B$ as shown in Fig. 6(b). It is assumed that the magnetizations lie in the $xz$ plane; the validity of this assumption will be examined later. It is convenient to refer the nonequilibrium components of the magnetization in each layer to its own rotated coordinate system such that the $\zeta$ direction is parallel with the equilibrium magnetization and $\xi,y$ specify directions which are orthogonal to the equilibrium magnetization. The magnetic free-energy contribution from each film can then be expanded to second order in the small variables $M_\xi, M_y$. As a further simplification we assume that the spatial variation of the magnetization density across the thickness of each film can be ignored for purposes of calculating the normal modes of the coupled two-layer system. This assumption, which corresponds to an infinite exchange stiffness along the $y$ direction, enormously simplifies the dynamic problem. The state of the two films can be specified by four dynamic amplitude variables: it is convenient to take these to be the magnetizations per unit area of film $m_{A\xi}=d_A M_{A\xi}$, $m_{Ay}=d_A M_{Ay}$, $m_{B\xi}=d_B M_{B\xi}$, and $m_{By}=d_B M_{By}$. The amplitudes $m_{A\xi}$ and so on depend upon time and may depend upon position in the $xz$ plane. As will be seen later, the assumption of uniform magnetization within each film along the specimen normal is probably not adequate for the calculation of BLS intensities.

In order to avoid extra complications with the notation we have used the same subscript symbols for the local axes in films $A$ and $B$. It must always be borne in mind that the components $m_{A\xi}$ and $m_{B\xi}$ are parallel only if the angles $\theta_A$ and $\theta_B$ are equal. The components $m_{Ay}$ and $m_{By}$ are always parallel.

The free energy per unit area for the coupled bilayer

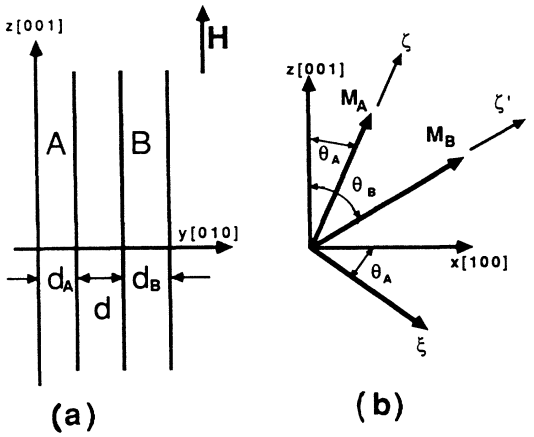


FIG. 6. Coordinate system used to describe the normal modes of thin exchange-coupled magnetic bilayers. In (a) the axes are assumed to be parallel with the cubic crystalline axes in each film. (b) illustrates the use of a local coordinate system which has been chosen so that the $\zeta$ axis lies along the direction of the equilibrium magnetization: the local coordinate axes are different for the two films $A$ and $B$.

system can be written as $F=F_H+F_c+F_M+F_S+F_X$, where the individual terms are discussed in sections (i)–(v). Only terms which are quadratic in small quantities have been kept and constant terms that are of no interest here have been suppressed.

(i) The free energy of interaction with the applied magnetic field,

$$F_H=-HM_A d_A\cos\theta_A-HM_B d_B\cos\theta_B+H\sin\theta_A m_{A\xi}+H\sin\theta_B m_{B\xi}+(H\cos\theta_A/2M_A d_A)(m_{A\xi}^2+m_{Ay}^2)+(H\cos\theta_B/2M_B d_B)(m_{B\xi}^2+m_{By}^2)\ . \tag{4}$$

(ii) The free energy per unit area due to the magnetocrystalline anisotropy,

$$F_c=(K_{A1}d_A/8)(1-\cos4\theta_A)+(K_{B1}d_B/8)(1-\cos4\theta_B)+(K_{A1}/2M_A)\sin4\theta_A m_{A\xi}+(K_{B1}/2M_B)\sin4\theta_B m_{B\xi}+(K_{A1}/d_A M_A^2)\cos4\theta_A m_{A\xi}^2+(K_{B1}/d_B M_B^2)\cos4\theta_B m_{B\xi}^2+(K_{A1}/4d_A M_A^2)(3+\cos4\theta_A)m_{Ay}^2+(K_{B1}/4d_B M_B^2)(3+\cos4\theta_B)m_{By}^2\ . \tag{5}$$

(iii) The free energy per unit area due to surface poles when the magnetization is tipped uniformly out of the plane,

$$F_M=(2\pi/d_A)m_{Ay}^2+(2\pi/d_B)m_{By}^2\ . \tag{6}$$

In writing Eq. (6) it has been assumed, for simplicity, that the appropriate demagnetizing factor is $4\pi$ corresponding to a film that is thick compared with its atomic spacing. For a discussion of this point, see the Appendix of Heinrich *et al.*[2]

(iv) Surface free energies due to the broken cubic symmetry at the film surfaces

$$F_S=-(K_{Au}/d_A^2M_A^2)m_{Ay}^2-(K_{Bu}/d_B^2M_B^2)m_{By}^2\ . \tag{7}$$

$K_{Au},B_{Bu}$ are uniaxial surface-energy parameters having units of ergs per unit area. Positive $K_{Au},K_{Bu}$ corresponds to effective fields that tend to rotate the magnetizations out of the plane.

(v) An exchange-coupling energy between the two ferromagnetic films having the form used by Hoffman *et al.*[3] [this is just Eq. (1) rewritten using the new variables],

$$F_X=J(\mathbf{m}_A\cdot\mathbf{m}_B)/(d_A M_A d_B M_B)\ . \tag{8}$$

For convenience the sign of this interaction has been chosen so that positive $J$ corresponds to an antiferromagnetic coupling. When expanded to second order in small variables this expression becomes

$$F_X=J\{\cos(\theta_B-\theta_A)+[\sin(\theta_B-\theta_A)/d_A M_A]m_{A\xi}+[\sin(\theta_A-\theta_B)/d_B M_B]m_{B\xi}+[\cos(\theta_B-\theta_A)/d_A M_A d_B M_B]m_{A\xi}m_{B\xi}+(1/d_A M_A d_B M_B)m_{Ay}m_{By}-[\cos(\theta_B-\theta_A)/2d_A^2M_A^2](m_{A\xi}^2+m_{Ay}^2)-[\cos(\theta_B-\theta_A)/2d_B^2M_B^2](m_{B\xi}^2+m_{By}^2)\}\ . \tag{8a}$$

### A. The equilibrium configuration

For a stable equilibrium, it is required that (1) the sum of the terms linear in $m_{A\xi},m_{B\xi}$ in the total free energy $F$ vanish, and that (2) $F$ has a positive-definite quadratic form in the variable pairs $m_{A\xi},m_{B\xi}$, and $m_{Ay},m_{By}$. Both of these conditions are algebraically complex. For films having the magnetic properties listed in Table II the free energy increases when the magnetizations are rotated out of the film plane for any value of the exchange-coupling parameters $J$, if the angles $\theta_A,\theta_B$ are chosen so as to satisfy condition (1) i.e., so that the coefficients of the linear terms in the total free energy vanish. This means that for this model and for a pair of films having the properties listed in Table II the equilibrium magnetizations remain parallel with the plane for all values of the applied magnetic field and for all values of the coupling parameter $J$.

For applied fields larger than a critical value $H_c$ the equilibrium magnetizations of each film remain parallel with the direction of the applied field (along a cubic axis) i.e., $\theta_A=\theta_B=0$. It is straightforward to show (from the condition that the derivatives of the free energy with respect to $\theta_A,\theta_B$ vanish) that for our model this critical field satisfies the condition

$$\left[H_c+\frac{2K_{A1}}{M_A}\right]\left[H_c+\frac{2K_{B1}}{M_B}\right]=J\left[\frac{H_c+\frac{2K_{A1}}{M_A}}{d_B M_B}\right]+J\left[\frac{H_c+\frac{2K_{B1}}{M_B}}{d_A M_A}\right]\ . \tag{9}$$

For films made of identical materials (i.e., $M_A=M_B=M_s$ and $K_{A1}=K_{B1}=K_1$) this inelegant equation becomes much simpler:

$$H_c=(J/M_s)\left[\frac{1}{d_A}+\frac{1}{d_B}\right]-(2K_1/M_s)\ . \tag{9a}$$

For applied fields less than the critical value the magnetizations $M_A$ and $M_B$ do not remain oriented along the direction of the external field and they do not remain parallel with each other because of the antiferromagnetic

coupling energy (8). The dependence of the equilibrium angles on the strength of the applied field can be quite complicated and depends explicitly on the properties of the two individual films. For example, for two identical films one must have $\theta_B = -\theta_A$ by symmetry so that as the strength of the external field is reduced the magnetizations rotate in opposite directions and finally in zero field become oriented at right angles to the field direction along an easy axis.[26] For comparison with FMR and BLS measurements we are interested in the asymmetrical case of two unequal films: the FMR absorption and the BLS scattering intensities vanish by symmetry for the optical mode in identical ultrathin films.[28] As an example, consider two iron films for which film $A$ has twice the thickness of film $B$, but the films are otherwise very similar (see Table II), the magnetic-field dependence of the equilibrium angles is shown in Fig. 7(a) and the component along the field direction of the total moment per unit area is shown in Fig. 7(b). These results were obtained numerically and for fields decreasing from a starting magnetic field that was greater than the critical field $H_c$ given by Eq. (9): Thus the magnetizations were initially parallel with each other and with the applied field. In this case the variation of the magnetization angles with field strength is quite complicated. At zero field the magnetization of the thickest film becomes aligned with the field direction, whereas the magnetization of the thinnest film rotates into a direction antiparallel with the field directions: both, of course, lie along an easy axis. The angles $\theta_A, \theta_B$ for a given field strength were determined from preceding condition (1), i.e., that the derivatives of the free energy with respect to these angles vanish at equilibrium. The search for the equilibrium angle was conducted by following the free-energy contours along the paths corresponding to steepest descent.[27]

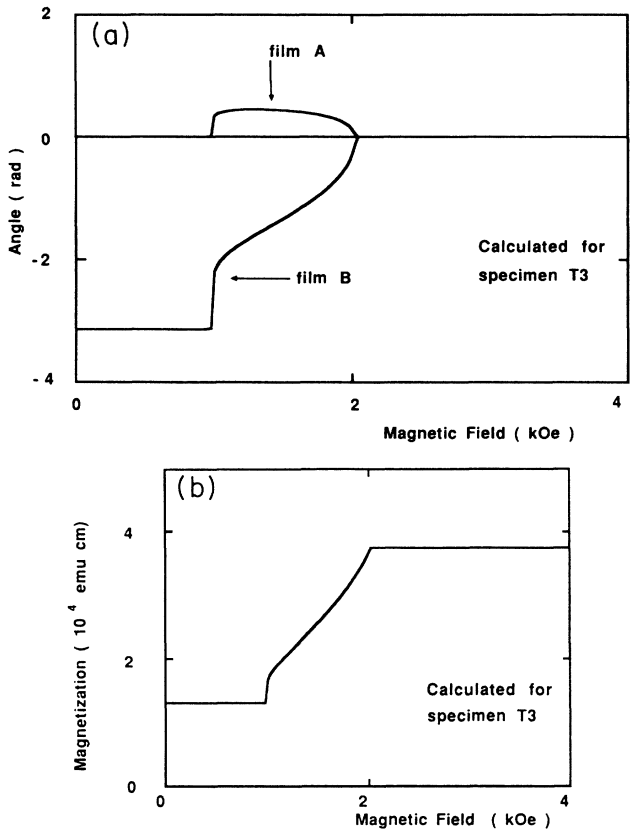


FIG. 7. (a) The applied magnetic-field variation of the equilibrium direction of the magnetizations for films $A$ and $B$ calculated for an antiferromagnetic exchange coupling between the films, $J=0.18$ ergs/cm$^2$. The model films are characterized by the parameters listed for specimen $T3$ in Table III. (b) The magnetic-field variation of the total component of magnetization along the applied field direction calculated for two films characterized by the parameters listed for specimen $T3$ in Table III. The films are assumed to be coupled by an antiferromagnetic exchange interaction having the strength $J=0.18$ ergs/cm$^2$. By definition $M_H = M_A \cos\theta_A + M_B \cos\theta_B$, where the field variation of $\theta_A, \theta_B$ is shown in (a).

### B. Oscillation around the directions of the equilibrium magnetizations

The magnetization waves measured in our BLS experiments can be characterized by a space and time variation of the form $\exp[i(qx - \omega t)]$. This is because the plane of incidence of the laser light was chosen to be perpendicular to the magnetic-field direction, as shown in Fig. 8. For the backscattering geometry[16,17] the wave vector in the plane is given by $q = \pm(2\omega_0/c)\sin\theta$, where $\omega_0$ is the frequency of the light, $\theta$ is its angle of incidence, and $c$ is the velocity of light. Each magnetization component must satisfy a Landau-Lifshitz equation of motion of the form

$$(i\omega/\gamma)m_{A\xi} = T_{A\xi} , \tag{10}$$

with similar equations for $m_{Ay}$, $M_{By}$, and $m_{B\xi}$. In Eq.

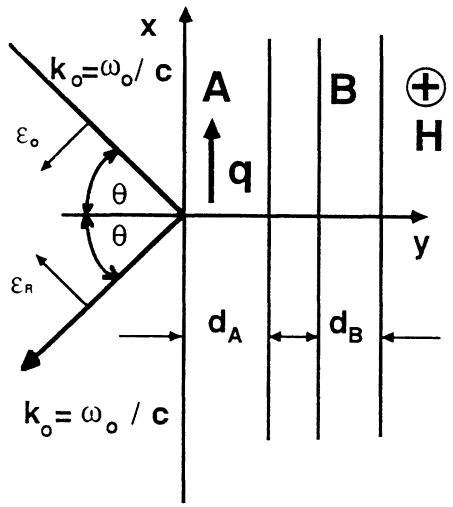


FIG. 8. This diagram illustrates the relationship between the optical scattering plane, the applied magnetic field $H$, and the magnon wave vector $q$, in the bilayer films $A,B$. The wave vector of the scattered light for the backscattering configuration is parallel with the wave vector of the incident light but reversed in direction.

(10) $T_{A\xi}$ is the component of torque along the $\xi$ direction [Fig. 6(b)] and $\gamma = g|e|/2mc$ is the spectroscopic splitting factor. Damping will not be included in the equations of motion: we are interested in integrated light-scattering intensities rather than in the spectral distribution of the scattered light. The torques that enter the equations of motion (10) can be attributed to the action of effective magnetic fields.[29] The most important of these effective fields are due to the variation of the free-energy terms, Eqs. (4)–(8), as the magnetization in each film is rotated away from equilibrium

$$h_{A\xi} = -(\partial F/\partial m_{A\xi}) , \tag{11}$$

with similar terms associated with the other three magnetization components. In addition one has intralayer exchange fields[30] and dipole fields due to the spatial variation of the magnetization along the $x$ direction. For film $A$ the intralayer exchange field components are given by

$$h_{A\xi} = -\left[\frac{2A_A q^2}{M_A^2}\right] m_{A\xi} , \tag{12a}$$

$$h_{Ay} = -\left[\frac{2A_A q^2}{M_A^2}\right] m_{Ay} , \tag{12b}$$

with similar expressions for film $B$. The dipole magnetic-field components have been written in Appendix A. Explicit expressions for the linearized Landau-Lifshitz equations of motion in which only terms linear in the magnetization amplitudes have been retained have been written in Appendix B.

The integrated intensity of the light scattered from a given magnetization mode has been calculated using a modification of the procedure described by Cochran and Dutcher.[31] In this approach the magnetization amplitudes associated with a given mode are calculated from the requirement that the mode energy be equal to the thermal average for a harmonic oscillator having the same frequency; in the present case this thermal average is just the value $kT$ corresponding to approximately 300 K ($4.14\times10^{-14}$ ergs). The precession of the thermally excited magnetization around its equilibrium position modulates the optical dielectric constant of the material. A $p$-polarized incident optical field which has $x,y$ components of the electric field (see Fig. 8) generates optical polarization densities given, in lowest order, by[32]

$$4\pi P_x = KE_y M_z , \tag{13a}$$

$$4\pi P_y = -KE_x M_z , \tag{13b}$$

$$4\pi P_z = KE_x M_y - KE_y M_x , \tag{13c}$$

where $K$ is the first order magneto-optic coupling parameter,[15,32] and where $M_x, M_y, M_z$ are time-dependent magnetization densities referred to the cubic axes of the crystal system that, in the present case, correspond to the $x,y,z$ laboratory axes (Figs. 6 and 8). The metal films with which we are concerned are very thin compared with the optical skin depths of iron, copper, and gold and therefore the spatial variation of the optical electric field can be ignored—not only within a given iron film but also between the two iron films.[33] Also relative scattering intensities rather than absolute intensities are of interest, therefore one can ignore the factors that describe the effect of optical interference on the amplitudes of the incident and scattered optical electric fields: these factors are in any case independent of the applied magnetic field in the approximation that we are using. With these simplifications, the ratio of the scattered-light amplitude to the incident-light amplitude can be written (for the backscattering configuration) (see Appendix C),

$$E_s/E_0 \sim m_{Ay} - [(\sin\theta/\cos\theta) m_{A\xi}\cos\theta_A] + m_{By} - [(\sin\theta/\cos\theta) m_{B\xi}\cos\theta_B] , \tag{14}$$

where $m_{A\xi}, m_{B\xi}, m_{Ay}, m_{By}$ are the magnetization amplitudes associated with the energy $kT$. For $p$-polarized incident light the scattered light is $s$ polarized, and for $s$-polarized incident light the scattered light is $p$ polarized. It can be shown by direct calculation that the ratio of the backscattered electric-field amplitude to the incident optical electric-field amplitude is proportional to the factor on the right-hand side of Eq. (14) independent of the polarization of the incident light (Appendix C).

## COMPARISON OF THE CALCULATIONS WITH EXPERIMENT

The calculation outlined in the previous section was compared with the results of experiments for the two magnetic bilayer specimens that exhibited two spin-wave modes: specimens $T3$ and $T4$ of Table I. The magnetic parameters listed for the iron films $S1$ and $S2$ of Table II were used for the individual iron films in the bilayers. It was found that a value for the exchange parameter could be found for which the calculated and measured field dependencies of the two spin-wave frequencies were in reasonable agreement. Small adjustments of the two uniaxial surface-energy parameters, $K_{Au}$ and $K_{Bu}$, together with a small adjustment of the exchange parameter, $J$, were used to procure a better agreement between theory and experiment. The results of this fitting procedure for specimen $T3$ are shown by the solid lines in Fig. 3. The three fitting parameters $J$, $K_{Au}$, and $K_{Bu}$ are interdependent but it was found that the magnetic-field scale of the low field variation shown in Fig. 3, as well as the frequency separation of the two modes, was particularly sensitive to the value chosen for $J$, whereas the other two parameters mainly affected the slopes of the high field frequency versus field curves: $K_{Au}$ affected primarily the high-frequency branch (the acoustic mode) whereas $K_{Bu}$ affected mainly the low-frequency branch (the optical mode). The same calculation was used to fit the data for bilayers $T1$ and $T2$, but using a negative value for the exchange-coupling parameter corresponding to ferromagnetic exchange. The frequency of the acoustic mode (the low-frequency branch in this case) is insensitive to the value of $J$ for large values of the coupling parameter. We were therefore not able to provide an estimate of $J$ for $T1$ and $T2$ from our data. For purposes of analysis we arbitrarily used the value $J = -10$ ergs/cm$^2$. This is a large coupling in the sense that the effective fields ($\sim J/d_A M_a$)

TABLE III. Parameters deduced from a comparison of theory with BLS data for the magnetic bilayer films $T1-T4$ of Table I. The saturation magnetization density has been taken to be that of bcc bulk iron at room temperature, $4\pi M_s = 21.55$ kOe. The factor 1 ML = 1.43 Å has been used to calculate the iron film thicknesses, $d$. $4\pi M_{\text{eff}} = 4\pi M_s - 2K_u/dM_s$. FM means ferromagnetic exchange coupling between the two films; AM means antiferromagnetic coupling. To obtain the effective interlayer exchange stiffness parameter $A^{AB}$ multiply $J$ by $a/4 = 7.14 \times 10^{-9}$ [Heinrich *et al.* (Ref. 2)]. The in-plane magnetic anisotropy fields are $2K_{A1}/M_A = 0.259$ kOe for film $A$ and $2K_{B1}/M_B = 0.113$ kOe for film $B$.

| | | Film $A$ | | | Film $B$ | | |
|---|---|---|---|---|---|---|---|
| Specimen | $J$ (ergs/cm$^2$) | $d$ (ML) | $4\pi M_{\text{eff}}$ (kOe) | $K_{Au}$ (ergs/cm$^2$) | $d$ (ML) | $4\pi M_{\text{eff}}$ (kOe) | $K_{Bu}$ (ergs/cm$^2$) |
| $T1$ | −10.0[a] (FM) | 11.0 | 14.28 | 0.98[b] | 5.0 | −1.28 | 1.40 |
| $T2$ | −10.0[a] (FM) | 9.5 | 13.14 | 0.98[b] | 5.0 | −0.47 | 1.35 |
| $T3$ | 0.18[c] (AF) | 10.3 | 12.84 | 1.10 | 5.0 | 2.30 | 1.18 |
| $T4$ | 0.14[d] (AF) | 9.0 | 13.39 | 0.90 | 4.8 | 3.03 | 1.09 |

[a]This value is arbitrary; it represents a large exchange coupling.
[b]This value is that found for the single layer $S1$; it is not possible for strongly coupled films to obtain $4\pi M_{\text{eff}}$ independently for each film. See the text.
[c]$J = 0.22$ ergs/cm$^2$ from FMR data (Ref. 1)
[d]$J = 0.14$ ergs/cm$^2$ from FMR data (Ref. 1)

produced by it are of the order of 40 kOe for a 10-ML-thick film. Magnetic parameters deduced for the four magnetic bilayer films that we studied are listed in Table III. Notice that the values for the effective magnetizations for films $T3$ and $T4$ required to fit the data are not very different from the effective magnetizations required to fit the single iron films (Table II). This indicates that the structure and quality of the films grown in the bilayer structures are very similar to the structure and quality of the single iron films.

The magnetic-field dependence of the scattered-light intensities for the two magnetic modes corresponding to sample $T3$ has been calculated: the results are displayed in Fig. 9. This figure should be compared with the experimentally observed intensities shown in Fig. 5. It is obvious that there are discrepancies between the observed and calculated intensities. The most obvious differences are (1) The intensity of the high-frequency mode was observed to become weak at small magnetic fields contrary to the calculation shown in Fig. 9. (2) The intensity of the low-frequency mode decreased rapidly with increasing field over the interval 0–2 kOe contrary to the predictions of the model.

The origin of these discrepancies is not known. It is very probable that our model, which assumes a uniform rotation of the equilibrium magnetizations, is too simple. It is interesting to note that if, for some reason, the magnetizations at zero applied field should become oriented along the easy axis that is perpendicular to the field direction (along the $x$ axis of Fig. 6), the calculated intensity of the BLS peak corresponding to the high-frequency mode would be reduced by the factor $\frac{1}{242}$ over the intensity at $H=0$ shown in Fig. 9. The intensity of the low-frequency mode would be reduced by only 30%. The frequencies at $H=0$ of the two modes would be slightly reduced (11.95 and 4.20 GHz versus the values 12.69 and 4.88 GHz shown in Fig. 3). However, the Kerr-effect measurements show that the total magnetization at low fields has precisely the value corresponding to magnetizations in the two films that are antiparallel but aligned along the applied field direction (see the inset of Fig. 4 of Heinrich *et al.*[1]). A comparison of the SMOKE results with the calculated field dependence of the magnetization shown in Fig. 7(b) reveals that the onset of the low field plateau, which is predicted to occur at 1 kOe, is observed to occur at a much smaller magnetic field—between 0.1 and 0.2 kOe. This indicates that the detailed manner in which the magnetizations in the two films transform from a parallel configuration at high fields to an antiparallel configuration at low fields is not described accurately by our simple model of exchange-coupled bilayers. Presumably the details of the transformation depend upon the distribution of surface irregularities that may affect the local value of the exchange-coupling parameter.

The ratio of the BLS intensities for the high- and low-frequency modes predicted for small applied fields, and therefore for antiparallel magnetizations aligned along the field direction, Fig. 9, is inverted relative to the observed intensity ratio. Specimens $T3$ and $T4$ (Table III)

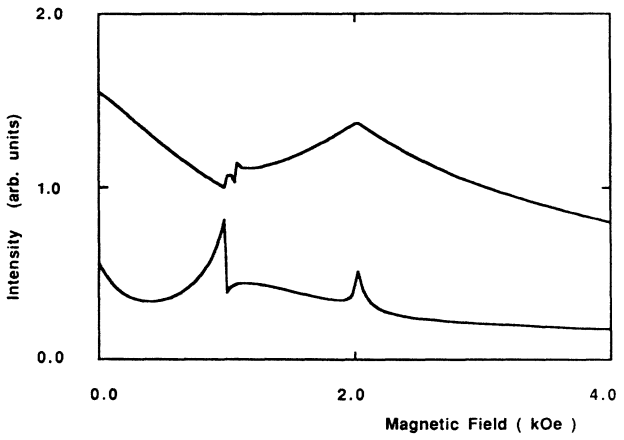


FIG. 9. The calculated magnetic-field dependence of BLS intensities for both the high- and low-frequency modes for two antiferromagnetically exchange-coupled thin films having the parameters listed for specimen $T3$ in Table III.

displayed two magnetic modes for each value of applied field: in each case in the limit of small fields the intensity of the low-frequency mode was found to be three to four times larger than the intensity of the high-frequency mode. We would like to understand the origin of the difference between calculated and observed low field BLS intensities because, in principle, these intensities carry information concerning the relative orientations of the static magnetizations in the two films. Moreover, the light-scattering experiment provides a probe that is only 20 $\mu$m in diameter: it could therefore be used to examine the magnetization distributions across the specimen.

It may be that the neglect of the spatial variation of the magnetization across each film is unwarranted. We have compared the simple rigid magnetization model with a more sophisticated calculation in which the magnetization in each film is allowed to vary across the thickness of the film.[22] Similar calculations have been described by Grünberg and co-workers[21,23] and by Hillebrands and co-workers.[24,25] These complex theories are only valid when the equilibrium magnetizations are parallel with each other and with the applied magnetic field. A comparison between the simple calculation, which assumes a rigid magnetization density across each film, and the complex calculation, which takes into account the finite exchange stiffness across each film, could only be carried out for fields larger than the critical value, Eq. (9). When applied to the case of bilayer $T3$ this implies that the comparison could only be carried out for fields larger than 2.03 kOe. For this example, frequencies calculated using the simple model were in agreement with those calculated using the complex model within 0.05 GHz for $q=1.73\times10^5$ cm$^{-1}$ (corresponding to 5145 Å light incident at 45°). For fields greater than 3 kOe both models predict a slow decrease of BLS intensities with increasing field. The complex model predicts a ratio of intensities for the two modes of 3:1 at 3 kOe (in agreement with experiment), whereas the simple model predicts an intensity ratio of 4:1.

It should also be mentioned that a detailed comparison of the two models indicates that the simplified treatment of dipole-dipole coupling between the two magnetic films is not adequate. Frequencies for both the high- and low-frequency modes calculated for $q=+1.73\times10^5$ cm$^{-1}$ were in agreement within 0.05 GHz for both the simple and the complex models.[37] However, for $q=-1.73\times10^5$ cm$^{-1}$, the high-frequency-mode frequencies calculated using the simple model were found to be approximately 2 GHz lower than frequencies calculated using the complex model for fields near 2 kOe: the discrepancy decreased with increasing magnetic field. The low-frequency-mode frequencies calculated using the two models were in agreement within 0.05 GHz. Frequencies calculated for wave vectors $+q$ and for $-q$ using the complex model were the same within 0.05 GHz: this result is in agreement with experiment since no difference in Stokes and anti-Stokes frequencies were observable for fields greater than 2 kOe. (The experimental uncertainty was approximately 0.8 GHz.)

The magnetic-field dependence of the mode frequencies calculated using the simple model of exchange-coupled magnetic bilayers previously described exhibits features that are very similar to those measured in the BLS experiments. This gives us confidence that the model can be used together with the experimental data to deduce meaningful values for the interlayer exchange-coupling parameter $J$. The excellent agreement between frequencies measured using BLS and the FMR data[1] for 36.3 GHz should be emphasized. The FMR measurement samples the specimens over dimensions of approximately 1 cm (the diameter of the resonant microwave cavity) whereas the BLS experiment samples the specimens over a length of approximately $10^{-3}$ cm (the diameter of the focused laser beam). The agreement between measurements made using these two very different length scales indicates that the magnetic properties of these films prepared by means of molecular-beam epitaxy are uniform. There is some evidence for a slow spatial variation of the exchange-coupling parameter $J$ from a comparison of FMR linewidths with the BLS linewidths. The FMR optical-mode linewidth was found to be approximately four times as large as the acoustic-mode linewidth[1] for specimen $T3$ (830 Oe versus 210 Oe). The BLS linewidths were observed to be approximately the same for both modes, and were equal to the instrumental resolution—approximately 0.8 GHz for a free spectral range of 30 GHz (see Fig. 4): this resolution is equivalent to an FMR linewidth of 270 Oe. The acoustic-mode frequency is insensitive to the value of the exchange-coupling parameter $J$, but the optical-mode frequency is very sensitive to the value of $J$. It appears, therefore, that the FMR optical-mode linewidth observed for specimen $T3$ was inhomogeneously broadened due to the spatial variation of $J$ over the specimen width: a 10% variation across the 1-cm-diam specimen would entirely account for the observed FMR linewidth. Such a slow spatial variation would not have any observable consequences for the BLS linewidths because of the small dimensions of the area sampled by the incident-light beam ($\sim10^{-3}$ cm).

## ACKNOWLEDGMENTS

The authors would like to thank the Natural Sciences and Engineering Research Council of Canada for the support which made this work possible.

## APPENDIX A: THE DIPOLE-DIPOLE COUPLING BETWEEN THE TWO THIN FILMS

Consider a single semi-infinite film of thickness $d$ whose surfaces are located at $y=-d/2$ and $y=+d/2$. Let the equilibrium magnetization be uniform and lie in the $xz$-plane, the plane of the film; it produces no poles. Let the components of the magnetization density which specify the deviation of the magnetization from equilibrium be

$$M_x(x)=M_x\exp(iqx) \quad \text{and} \quad M_y(x)=M_y\exp(iqx)\ . \tag{A1}$$

This magnetization distribution produces magnetic poles, and these poles generate a magnetic field. If one uses a scalar potential such that $\mathbf{h}=-\text{grad}\,V$ then

$$\nabla^2V=4\pi\,\text{div}\mathbf{M}=4\pi iqM_x\exp(iqx) \tag{A2}$$

inside the film, and $\nabla^2 V=0$ outside the film.[38] The solution of this standard boundary value problem gives the following field distributions.

(i) Inside the film,

$$h_x=[2\pi M_x e^{-qd/2}(e^{qy}+e^{-qy}) -4\pi M_x-2\pi i M_y e^{-qd/2}(e^{qy}-e^{-qy})]e^{iqx} , \quad \text{(A3a)}$$

$$h_y=[-2\pi i M_x e^{-qd/2}(e^{qy}-e^{-qy}) -2\pi M_y e^{-qd/2}(e^{qy}+e^{-qy})]e^{iqx} . \quad \text{(A3b)}$$

(ii) To the right of the film ($y \geq d/2$),

$$h_x=2\pi(M_x+iM_y)(e^{-qd/2}-e^{qd/2})e^{(-qy+iqx)} \quad \text{(A4a)}$$

$$h_y=2\pi(iM_x-M_y)(e^{-qd/2}-e^{qd/2})e^{(-qy+iqx)} . \quad \text{(A4b)}$$

(iii) To the left of the film ($y \leq -d/2$),

$$h_x=2\pi(M_x-iM_y)(e^{-qd/2}-e^{qd/2})e^{(qy+iqx)} , \quad \text{(A5a)}$$

$$h_y=-2\pi(iM_x+M_y)(e^{-qd/2}-e^{qd/2})e^{(qy+iqx)} . \quad \text{(A5b)}$$

These equations can be expanded in the small parameters $qy, qd$. Since $qd \ll 1$ it is sufficient to keep only the first-order terms. The terms in (A3) which are linear in $y$ give rise to magnetic torque terms which, to lowest order, average to zero when integrated across the film: they may therefore be ignored. With this simplification, one obtains to lowest order in $qd$ the following.

(i) Inside the film,

$$h_x=-2\pi M_x qd e^{iqx} , \quad \text{(A6a)}$$

$$h_y=-4\pi M_y[1-(qd/2)]e^{iqx} . \quad \text{(A6b)}$$

(ii) For $y \geq d/2$,

$$h_x=-2\pi qd(M_x+iM_y)e^{iqx} , \quad \text{(A7a)}$$

$$h_y=-2\pi qd(iM_x-M_y)e^{iqx} . \quad \text{(A7b)}$$

(iii) For $y \leq -d/2$,

$$h_x=-2\pi qd(M_x-iM_y)e^{iqx} , \quad \text{(A8a)}$$

$$h_y=2\pi qd(iM_x+M_y)e^{iqx} . \quad \text{(A8b)}$$

In applying these equations to the bilayer system of Fig. 6 it must be remembered that for film $A$ $M_{Ax}=M_{A\xi}\cos\theta_A$ and for film $B$ $M_{Bx}=M_{B\xi}\cos\theta_B$. Moreover, the small oscillatory fields of Eqs. (A6)–(A8) must be resolved into components in the $(\xi,y,\zeta)$ system for the appropriate film. Thus, dropping the term $e^{iqx}$ for convenience, one finds the following.

(a) Within film $A$,

$$h_{A\xi}=-2\pi qd_A M_{A\xi}(\cos\theta_A)^2 -2\pi qd_B(M_{B\xi}\cos\theta_A\cos\theta_B-iM_{By}\cos\theta_A) ,$$

$$h_{Ay}=-4\pi M_{Ay}+2\pi qd_A M_{Ay}+2\pi qd_B(iM_{B\xi}\cos\theta_B+M_{By}) .$$

(b) Within film $B$,

$$h_{B\xi}=-2\pi qd_B M_{B\xi}(\cos\theta_B)^2 -2\pi qd_A(M_{A\xi}\cos\theta_A\cos\theta_B+iM_{Ay}\cos\theta_B) ,$$

$$h_{By}=-4\pi M_{By}+2\pi qd_B M_{By}-2\pi qd_A(iM_{A\xi}\cos\theta_A-M_{Ay}) .$$

These fields produce the following first-order contributions to the torques per unit area:

$$T_{A\xi}=4\pi M_A m_{Ay}-2\pi M_A qd_A m_{Ay} -2\pi M_A qd_A(im_{B\xi}\cos\theta_B+m_{By}) , \quad \text{(A9)}$$

$$T_{Ay}=-2\pi M_A qd_A(\cos\theta_A)^2 m_{A\xi} -2\pi M_A qd_A(m_{B\xi}\cos\theta_A\cos\theta_B-im_{By}\cos\theta_A) , \quad \text{(A10)}$$

$$T_{B\xi}=4\pi M_B m_{By}-2\pi M_B qd_B m_{By} +2\pi M_B qd_B(im_{A\xi}\cos\theta_A-m_{Ay}) , \quad \text{(A11)}$$

$$T_{By}=-2\pi M_B qd_B(\cos\theta_B)^2 m_{B\xi} -2\pi M_B qd_B(m_{A\xi}\cos\theta_A\cos\theta_B+im_{Ay}\cos\theta_B) . \quad \text{(A12)}$$

In the preceding expressions $m_{A\xi}=d_A M_{A\xi}$, $m_{B\xi}=d_B M_{B\xi}$, and so on. It should be noted that the first terms in (A9) and in (A11) are also given by the effective fields calculated from the free-energy contribution (6): these torque contributions should not be counted twice.

## APPENDIX B: LINEARIZED EQUATIONS OF MOTION

The linearized equations of motion for the small magnetization amplitudes that specify the displacements of the magnetizations from equilibrium are given by

$$\left[\frac{i\omega}{\gamma_A}\right]m_{A\xi}=\left[H\cos\theta_A+\left[\frac{K_{A1}}{2M_A}\right](3+\cos4\theta_A)-\left[\frac{2K_{Au}}{d_A M_A}\right]+4\pi M_A\left[1-\frac{qd_A}{2}\right]-\frac{J\cos(\theta_B-\theta_A)}{d_A M_A}+\frac{2A_A q^2}{M_A}\right]m_{Ay} -2\pi M_A qd_A\cos\theta_B(im_{B\xi})+\left[\frac{J}{d_B M_B}-2\pi M_A qd_A\right]m_{By} , \quad \text{(B1)}$$

$$\left[\frac{i\omega}{\gamma_A}\right]m_{Ay}=-\left[H\cos\theta_A+\left[\frac{2K_{A1}}{M_A}\right]\cos4\theta_A+2\pi M_A qd_A(\cos\theta_A)^2-\frac{J\cos(\theta_B-\theta_A)}{d_A M_A}+\frac{2A_A q^2}{M_A}\right]m_{A\xi} -\left[\frac{J\cos(\theta_B-\theta_A)}{d_B M_B}+2\pi M_A qd_A\cos\theta_A\cos\theta_B\right]m_{B\xi}+i2\pi M_A qd_A\cos\theta_A m_{By} , \quad \text{(B2)}$$

$$\left[\frac{i\omega}{\gamma_B}\right]m_{B\xi}=2\pi M_B q d_B\cos\theta_A(im_{A\xi})+\left[\frac{J}{d_A M_A}-2\pi M_B q d_B\right]m_{Ay}$$
$$+\left[H\cos\theta_B+\left[\frac{K_{B1}}{2M_B}\right](3+\cos4\theta_B)-\left[\frac{2K_{Bu}}{d_B M_B}\right]+4\pi M_B\left[1-\frac{qd_B}{2}\right]-\frac{J\cos(\theta_B-\theta_A)}{d_B M_B}+\frac{2A_B q^2}{M_B}\right]m_{By}\ , \tag{B3}$$

$$\left[\frac{i\omega}{\gamma_B}\right]m_{By}=-\left[\frac{J\cos(\theta_B-\theta_A)}{d_A M_A}+2\pi M_B q d_B\cos\theta_A\cos\theta_B\right]m_{A\xi}-i2\pi M_B q d_B\cos\theta_B m_{Ay}$$
$$-\left[H\cos\theta_B+\left[\frac{2K_{B1}}{M_B}\right]\cos4\theta_B+2\pi M_B q d_B(\cos\theta_B)^2-\frac{J\cos(\theta_B-\theta_A)}{d_B M_B}+\frac{2A_B q^2}{M_B}\right]m_{B\xi}\ . \tag{B4}$$

It must be remembered that these magnetization components have been referred to local coordinate systems that are different for the two films (see Fig. 6).

## APPENDIX C: INTENSITY OF LIGHT SCATTERED FROM A THIN FILM

The polarization density induced in a thin film by an incident optical plane wave will be uniform if the film is very thin compared with the optical skin depth (typically $\sim 100$ Å). The time variation of the polarization density, $4\pi\mathbf{P}$, constitutes a current sheet that radiates an optical wave, i.e., the scattered light. For a film that is very thin compared with a wavelength of light, all parts of this current sheet radiate in phase. One can estimate the intensity of the radiated light by treating the polarization sheet like a $\delta$-function source of strength $4\pi\mathbf{P}d$, where $d$ is the film thickness. The fields radiated by a $\delta$-function current sheet can be written as follows (Cochran and Dutcher[31]):

(a) We write

$$4\pi P_x=\delta(y)\exp[i(Qx-\omega t)]\ .$$

This generates a $p$-polarized wave whose magnetic vector is polarized along $z$, Fig. 8. Its amplitude is given by

$$h_z^{(x)}=(i\omega/2c)\exp[i(Qx-ky-\omega t)]\ . \tag{C1}$$

(b) We write

$$4\pi P_y=\delta(y)\exp[i(Qx-\omega t)]\ .$$

This generates a $p$-polarized wave whose magnetic vector is given by

$$h_z^{(y)}=(i\omega/2c)\left[\frac{\sin\theta}{\cos\theta}\right]\exp[i(Qx-ky-\omega t)]\ , \tag{C2}$$

where $\theta$ is the angle of incidence (Fig. 8).

(c) We write

$$4\pi P_z=\delta(y)\exp[i(Qx-\omega t)]\ .$$

This polarization generates $s$-polarized light whose electric field is polarized along $z$, and whose amplitude is given by

$$E_z=(i\omega/2c)(1/\cos\theta)\exp[i(Qx-ky-\omega t)]\ . \tag{C3}$$

In the preceding expressions $\omega$ is the frequency of the scattered light: it is very nearly equal to the frequency of the incident light so that one may write with very little error $Q=(\omega/c)\sin\theta$ and $k=(\omega/c)\cos\theta$.

For $p$-polarized incident light the electric-field components are related to the angle of incidence of the light by (see Fig. 8)

$$E_x=-E_0\cos\theta\ , \tag{C4a}$$

$$E_y=-E_0\sin\theta\ . \tag{C4b}$$

It follows from (13a) and (13b) and from (C1) and (C2) that the amplitude of the $p$-polarized scattered light must vanish for any angle of incidence. For $p$-polarized incident light it is only the $z$ component of polarization density, see (13c), that generates a scattered wave, and this wave is $s$ polarized. According to (C3) and (C4), and using (13c), the amplitude of this $s$-polarized wave can be written

$$E_s\sim M_y-M_x\left[\frac{\sin\theta}{\cos\theta}\right]\ , \tag{C5}$$

or making use of the proportionality between $M_x,M_y$ and $m_x=M_x d$, $m_y=M_y d$ for a film uniformly magnetized across its thickness, one can write

$$E_s\sim m_y-m_x\left[\frac{\sin\theta}{\cos\theta}\right]\ . \tag{C6}$$

All that is now required in order to obtain Eq. (14) is to express the magnetization components in each film in terms of the natural variables $m_\xi,m_y$ (see Fig. 6) and to sum the contributions from film $A$ and from film $B$. Of course, one retains only terms which are linear in the small amplitudes $m_\xi,m_y$.

For $s$-polarized incident light the electric field is polarized along $z$ in the coordinate system of Fig. 8. In lowest order, this electric field generates $x,y$ components of the polarization density given by

$$4\pi P_x=-KM_y E_z\ , \tag{C7a}$$

$$4\pi P_y = K M_x E_z \ , \tag{C7b}$$

$$4\pi P_z = 0 \ , \tag{C7c}$$

From (C1) and (C2) the scattered light resulting from these polarizations will be $p$ polarized, and it will have an amplitude

$$h_z = E_p \sim m_y - m_x \left[ \frac{\sin\theta}{\cos\theta} \right] . \tag{C8}$$

Relation (C8) has the same form as (C6), which describes the amplitude of the $s$-polarized electric field generated by an incident $p$-polarized electric field.


*Permanent address: Physics Department, McGill University, Montreal, Quebec, Canada H3A 2T8.

[1]B. Heinrich, Z. Celinski, J. F. Cochran, W. B. Muir, J. Rudd, Q. M. Zhong, A. S. Arrott, K. Myrtle, and J. Kirschner, Phys. Rev. Lett. **64**, 673 (1990).

[2]B. Heinrich, S. T. Purcell, J. R. Dutcher, K. B. Urquhart, J. F. Cochran, and A. S. Arrott, Phys. Rev. B **38**, 12 879 (1988).

[3]F. Hoffman, A. Stankoff, and H. Pascard, J. Appl. Phys. **41**, 1022 (1970).

[4]The parameter $J$ in Eq. (1) should not be confused with the pair interaction energy commonly used to describe the nearest-neighbor exchange energy between localized spins. In the notation used in Ref. 2, $J=(4A^{AB}/a)$ where $A^{AB}$ is an interface exchange stiffness parameter and $a$ is the bcc lattice cube edge.

[5]A. G. Gurevich, *Ferrites at Microwave Frequencies* (Consultants Bureau, New York, 1963).

[6]P. A. Grünberg, J. Appl. Phys. **51**, 4338 (1980).

[7]P. A. Grünberg, J. Appl. Phys. **52**, 6824 (1981).

[8]R. L. Lyles, Jr., S. J. Rothman, and W. Jager, Metallography **11**, 363 (1978).

[9]B. Heinrich, K. B. Urquhart, A. S. Arrott, J. F. Cochran, K. Myrtle, and S. T. Purcell, Phys. Rev. Lett. **59**, 1756 (1987).

[10]B. Heinrich, A. S. Arrott, J. F. Cochran, K. B. Urquhart, K. Myrtle, Z. Celinski, and Q. M. Zhong, Mater. Res. Soc. Symp. Proc. **151**, 177 (1989).

[11]B. Heinrich, J. F. Cochran, A. S. Arrott, S. T. Purcell, K. B. Urquhart, J. R. Dutcher, and W. F. Egelhoff, Jr., Appl. Phys. A **49**, 473 (1989).

[12]Z. Q. Wang, S. H. Liu, Y. S. Li, F. Jona, and P. M. Marcus, Phys. Rev. B **35**, 9322 (1987).

[13]A. S. Arrott, B. Heinrich, and S. T. Purcell, in *Kinetics of Ordering and Growth at Surfaces,* edited by M. G. Legally (Plenum, New York, in press).

[14]W. F. Egelhoff, Jr. (private communication). See also W. F. Egelhoff, Jr. and I. Jacob, Phys. Rev. Lett. **62**, 921 (1988).

[15]J. R. Sandercock, in *Light Scattering in Solids II,* edited by M. Cardona and G. Güntherodt, Vol. 51 of *Topics in Applied Physics* (Springer, Berlin, 1982), Chap. 6.

[16]P. A. Grünberg, Prog. Surf. Sci. **18**, 1 (1985).

[17]P. A. Grünberg, in *Light Scattering in Solids V,* edited by M. Cardona and G. Güntherodt, Vol. 66 of *Topics in Applied Physics* (Springer, Berlin, 1989), Chap. 8.

[18]Newport Instruments Corp., Fountain Valley, California.

[19]J. G. Gay and R. Richter, Phys. Rev. Lett. **56**, 2728 (1986); J. Appl. Phys. **61**, 3362 (1987).

[20]J. F. Cochran, B. Heinrich, A. S. Arrott, K. B. Urquhart, J. R. Dutcher, and S. T. Purcell, J. Phys. (Paris) Colloq. **49**, C8-1671 (1988).

[21]J. Barnaś and P. Grünberg, J. Magn. Magn. Mater. **82**, 186 (1989).

[22]J. F. Cochran and J. R. Dutcher, J. Appl. Phys. **64**, 6092 (1988).

[23]M. Vohl, J. Barnaś, and P. Grünberg, Phys. Rev. B **39**, 12 003 (1989).

[24]B. Hillebrands, P. Baumgart, and G. Güntherodt, Appl. Phys. A **49**, 589 (1989).

[25]B. Hillebrands, Phys. Rev. B **41**, 530 (1990).

[26]J. J. Krebs, P. Lubitz, A. Chaiken, and G. A. Prinz, Phys. Rev. Lett. **63**, 1645 (1989).

[27]B. Dieny, J. P. Gavignan, and J. P. Rebouillat, Mater. Res. Soc. Symp. Proc. **151**, 35 (1989).

[28]The FMR absorption becomes very small for identical films whose thicknesses are small compared with the microwave skin depth. The BLS scattering intensities become very small for films having identical magnetic properties and which are thin compared with the optical skin depth.

[29]J. R. Macdonald, Proc. Phys. Soc. London **A64**, 968 (1951).

[30]W. F. Brown, Jr., *Micromagnetics* (Robert E. Kriegler Co., Huntington, New York, 1978), Chap. 3.

[31]J. F. Cochran and J. R. Dutcher, J. Magn. Magn. Mater. **73**, 299 (1988).

[32]W. Wettling, M. G. Cottam, and J. R. Sandercock, J. Phys. C **8**, 211 (1975).

[33]A calculation has been carried through for a 5-ML Fe film [$\varepsilon=(-0.4+i16.41)$] deposited on a Ag substrate [$\varepsilon=(-10.66+i0.33)$], then followed by 12 ML of Cu [we have used $\varepsilon=(-5.33+i6.18)$ appropriate for fcc Cu], 10 ML of Fe, and covered by 20 ML of Au [$\varepsilon=(-3.75+i2.75)$]. The electric-field amplitude decreased by approximately 6% across the 10-ML iron film and by approximately 2% across the 5-ML iron film. The discontinuity in the electric-field amplitude between the rear surface of the 10-ML film and the front surface of the 5-ML film was calculated to be 7%. Dielectric constants for 5145-Å light were obtained from Johnson and Christy (Refs. 34 and 35) for Ag, Cu, and Fe, and from Joensen *et al.* (Ref. 36) for Au.

[34]P. B. Johnson and R. W. Christy, Phys. Rev. B **6**, 4370 (1972).

[35]P. B. Johnson and R. W. Christy, Phys. Rev. B **9**, 5056 (1974).

[36]P. Joensen, J. C. Irwin, J. F. Cochran, and A. E. Curzon, J. Opt. Soc. Am. **63**, 1556 (1973).

[37]Positive $q$ corresponds to scattered light whose frequency has been increased by the magnon frequency; negative $q$ corresponds to scattered light whose frequency has been decreased by the magnon frequency.

[38]R. W. Damon and J. R. Eshbach, J. Phys. Chem. Solids **19**, 308 (1961).